Supporting information

Designing the tungsten sulfide blended perovskite anchored carbon nanotube composites for the high-performance supercapacitor

Sajjad Hussain[1a, b], Zulfqar Ali Sheikh[1c], K. Karuppasamy[d,e], Ghazanfar Nazir[b], Abdullah A. Al-Kahtani[f], Hyun-Seok Kim[g], Deok-Kee Kim[c], Jongwan Jung[a,b], Akram Alfantazi[d,e], Dhanasekaran Vikraman[g]*

[a] Hybrid Materials Center (HMC), Sejong University, Seoul 05006, Korea

[b] Department of Nanotechnology and Advanced Materials Engineering, Sejong University, Seoul 05006, Korea

[c] Department of Convergence Engineering for Intelligent Drone and Department of Electrical Engineering, Sejong University, Seoul 05006, Korea

[d.] Emirates Nuclear Technology Center (ENTC), Khalifa University of Science and Technology, Abu Dhabi, 127788, United Arab Emirates.

[e.] Department of Chemical and Petroleum Engineering, Khalifa University of Science and Technology, Abu Dhabi, 127788, United Arab Emirates.

[f] Department of Chemistry, College of Science, King Saud University, P.O. Box 2455, Riyadh 11451, Saudi Arabia

[g] Division of Electronics and Electrical Engineering, Dongguk University-Seoul, Seoul 04620, Korea

[1]Authors have contributed equally.

*Corresponding author's Email: v.j.dhanasekaran@gmail.com

S1. Chemicals

Iron(III) nitrate ($Fe(NO_3)_3.9H_2O$), sodium tungstate (Na_2WO_4), magnesium(II) nitrate ($Mg(NO_3)_2.4H_2O$), hydrochloride acid (HCl), Urea (H_2NCONH_2), hydrogen peroxide (H_2O_2), N-Methyl-2-pyrrolidone (NMP), sodium sulfide (Na_2SO_4), polyvinylidene difluoride (PVDF) activated carbon (AC), and acetonitrile were procured from Sigma-Aldrich. Commercial CNTs were purchased from the Sigma-Aldrich, Korea with the purity of >95%, a diameter range of 10–20 nm, a length of 5–15 μm and consist of 5–10 walls.

S2. Materials Characterizations

X-ray powder diffraction (XRD) was conducted with Cu-Kα radiation (0.154 nm) at 40 kV and 40 mA in the scanning range of 5-80° (2θ). Field emission scanning electron microscopy (FESEM) images and energy-dispersive X-ray spectroscopy (EDX) mapping images were obtained using (HITACHI S-4700), 5 kV. The Raman spectroscopy measurements were accomplished using Renishaw Invia RE04, Ar laser - 512 nm at room temperature. The morphology and microstructure of the samples were investigated by using high-resolution TEM (HRTEM, JEOL JEM-2100F, 200 kV). The X-ray photoelectron spectroscopy (XPS) measurement was recorded on an Ulvac PHI X-tool spectrometer with Al K_α X-ray radiation (1486.6 eV) to determine the surface properties of the as-prepared samples. XPS binding energies were calibrated using the C 1s peak at 284.8 eV as an internal reference. The BET specific surface area of the samples was analyzed by 3Flex surface characterization analyzer for nitrogen adsorption and desorption measurement at 77 K (Micromeritics, USA).

S3. Energy storage equations

The specific capacity ($C \cdot g^{-1}$) of the charge-discharge curve was determined by equation (S1):

$$Q(C.g^{-1}) = \frac{I \times \Delta t}{w} \quad \text{(S1)}$$

Δt is the discharge time, s; Q($C \cdot g^{-1}$) is the specific capacity; *I* refers to the discharge current, A; *w* resembles the mass of the loaded material, mg.

The specific capacity ($mAh \cdot g^{-1}$) of the charge-discharge curve was determined by equation (S2):

$$Q(mAh.g^{-1}) = \frac{I \times \Delta t}{3.6 \times w} \quad \text{(S2)}$$

Δt is the discharge time, s; Q($mAh \cdot g^{-1}$) is the specific capacity; *I* refers to the discharge current, A; *w* resembles the mass of the loaded material, mg.

The specific capacitance (C) was valued by the relation (S3):

$$C = \frac{i\,(\Delta t)}{w(\Delta V)} \quad \text{(S3)}$$

Δt is the discharge time, s; C is the specific capacitance, $F \cdot g^{-1}$; *I* refers to the discharge current, A; *w* resembles the mass of the loaded material, mg.

The optimal mass ratio of electrodes was determined using charge balance theory ($q^+ = q^-$), which extensively increases the electrochemical behavior of the ASC device. The mass ratio was determined by using the ensuing equation:

$$\frac{w_+}{w_-} = \frac{C_- \times V_-}{C_+ \times V_+}, \quad \text{(S4)}$$

where *w* refers to mass, C is the specific capacity and V refers to potential window.

The specific energy (E) and specific power (P) of the ASC devices were computed engaging the following formulas: WMC-2 ASC was extracted using the following relationships:

$$E = \frac{C_{ASC} \times (\Delta V)^2}{2 \times 3.6} \quad \text{(S5)}$$

$$P = \frac{E}{\Delta t} \quad \text{(S6)}$$

where *E*, *Δt* and *P* signify the specific energy, discharge time and specific power.

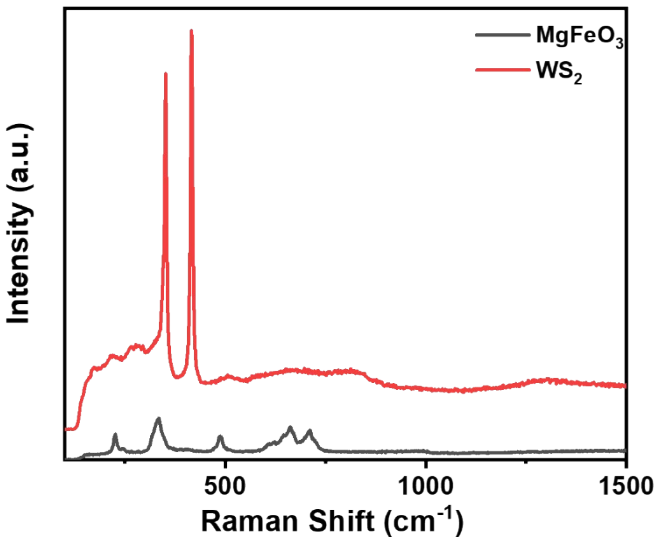

Figure S1. Raman spectra of $MgFeO_3$ and WS_2.

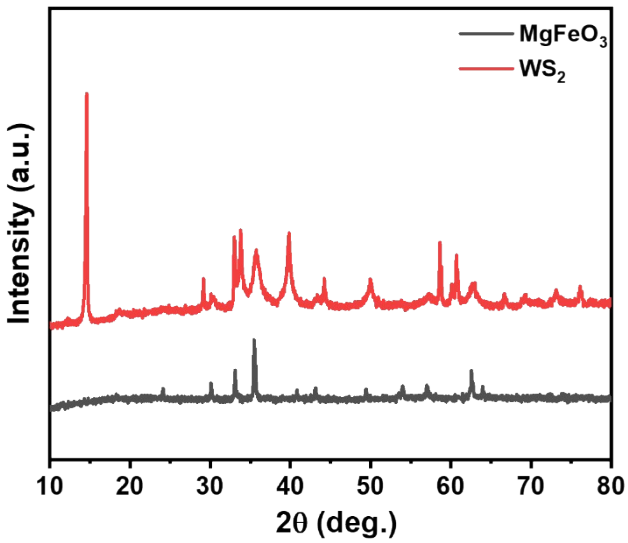

Figure S2. XRD spectra of $MgFeO_3$ and WS_2.

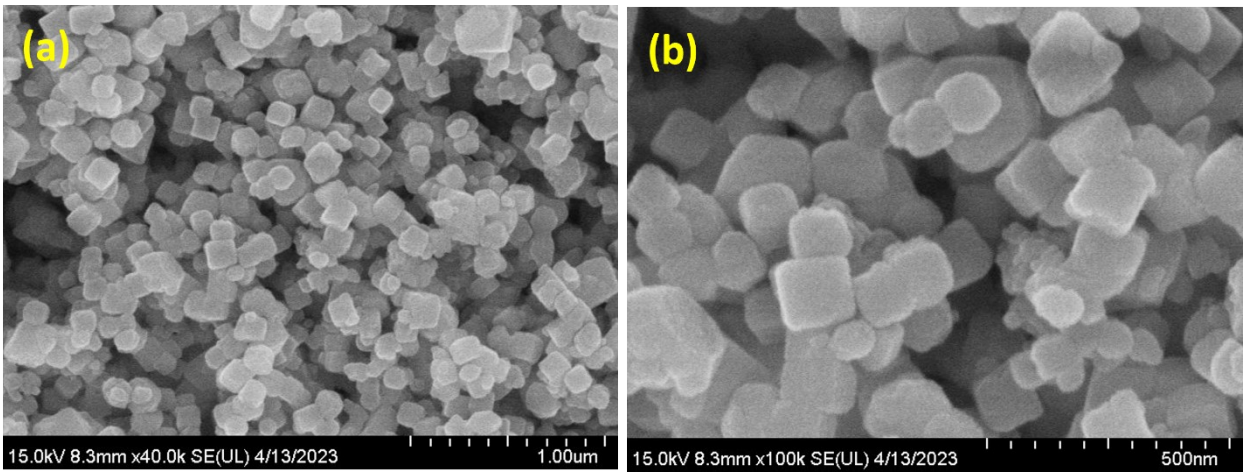

Figure S3. (a-b) FESEM micrographs of $MgFeO_3$ at different magnifications.

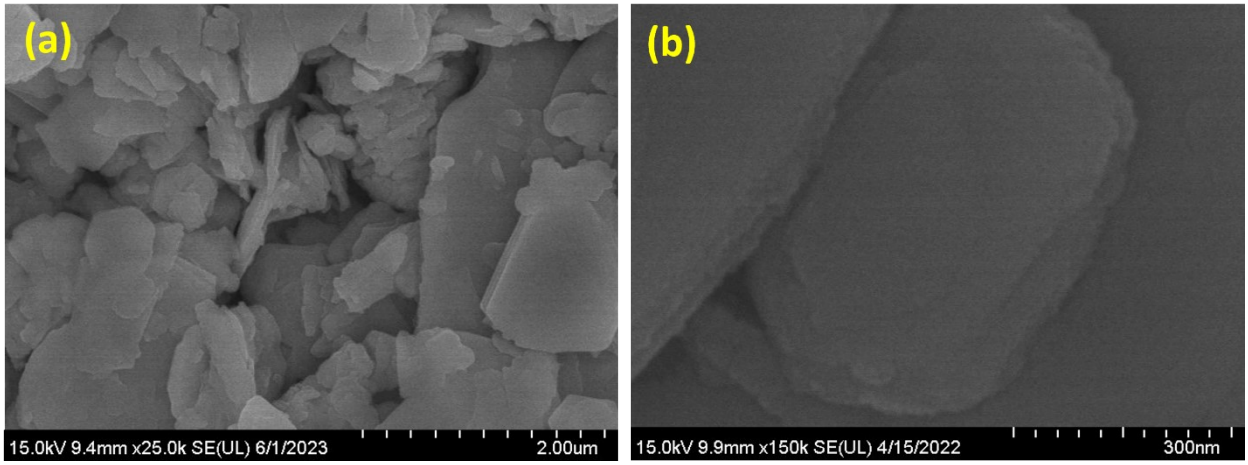

Figure S4. (a-b) FESEM micrographs of WS_2 at different magnifications.

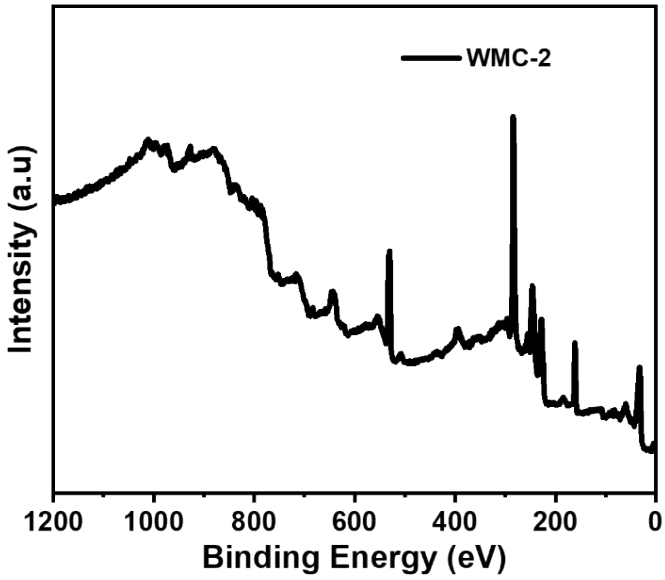

Figure S5. XPS survey spectrum of WMC-2 WS_2/$MgFeO_3$-CNT hybrid composite.

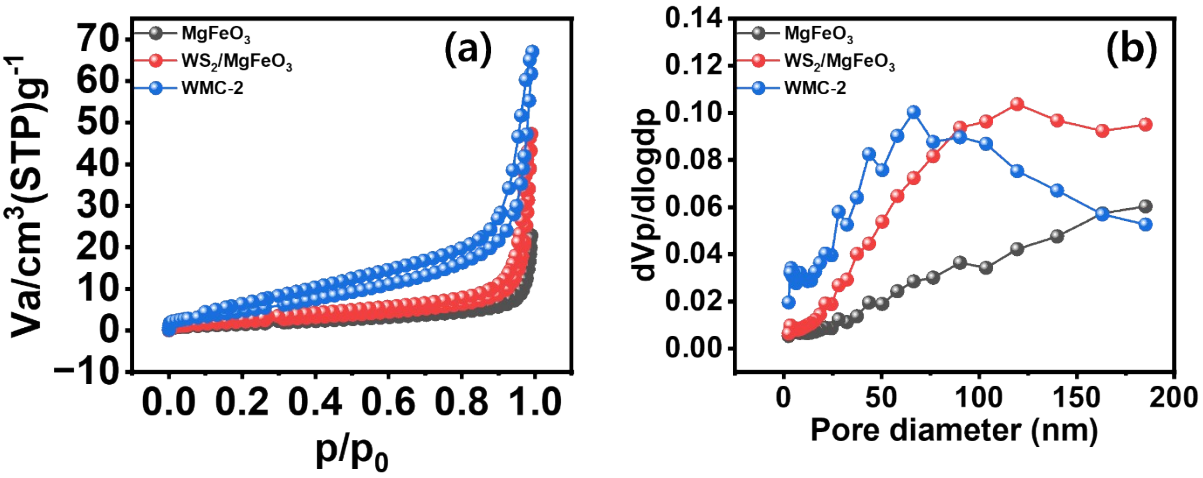

Figure S6. (a) BET and (b) BJH profiles for the $MgFeO_3$, $WS_2/MgFeO_3$ and WMC-2 hybrid composite.

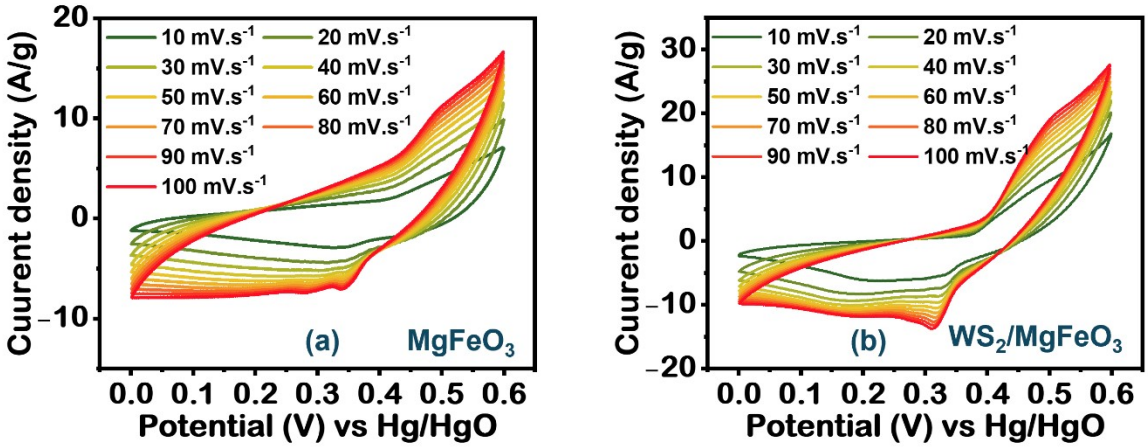

Figure S7. CVs at various scan rates for (a) $MgFeO_3$ and (b) $WS_2/MgFeO_3$ electrodes.

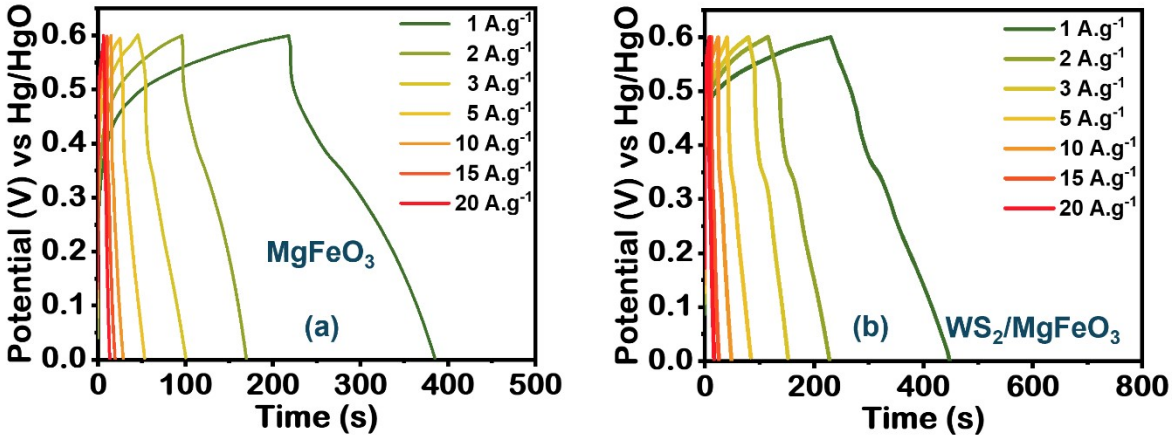

Figure S8. GCDs at various current densities for (a) $MgFeO_3$ and (b) $WS_2/MgFeO_3$ electrodes.

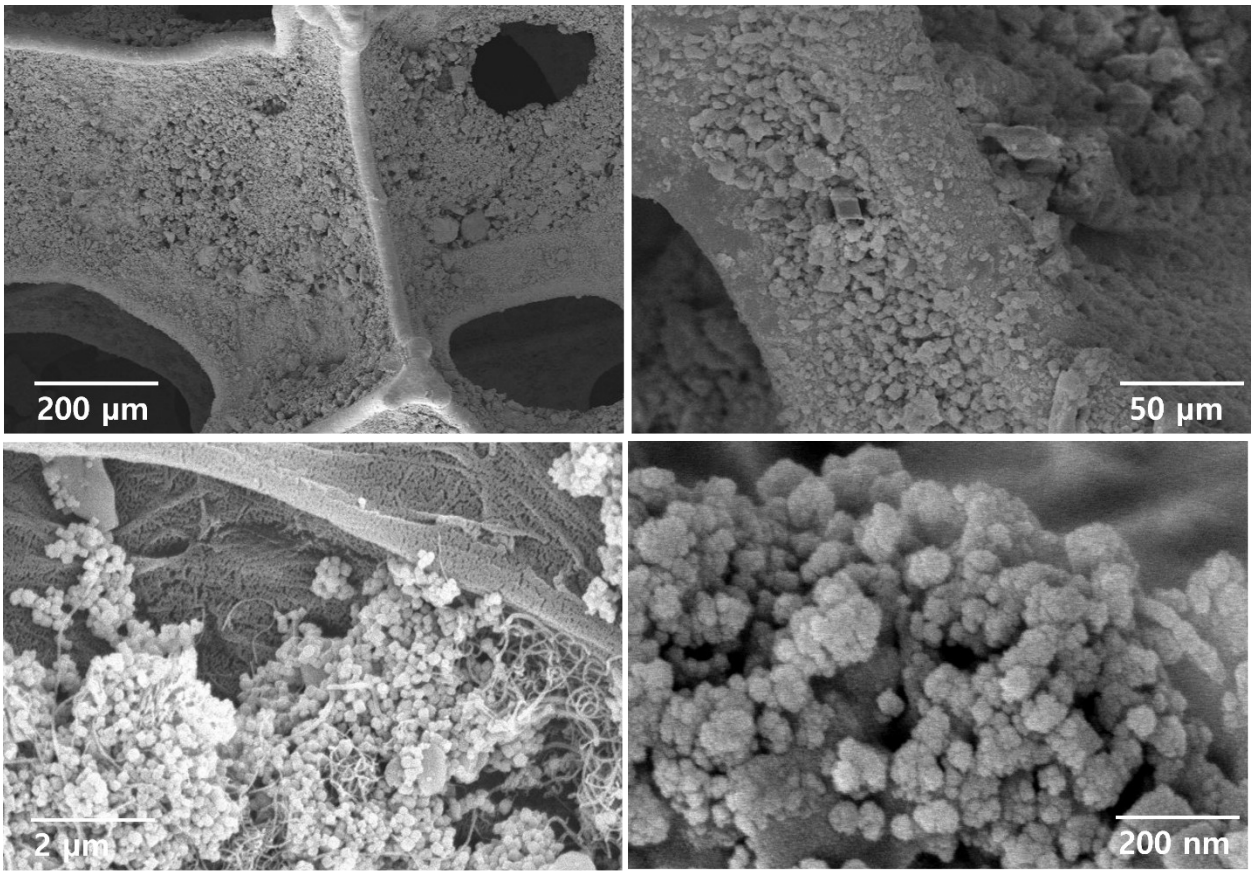

Figure S9. SEM images of WMC-2 $WS_2/MgFeO_3$-CNT on NF after 5000 cycling process.

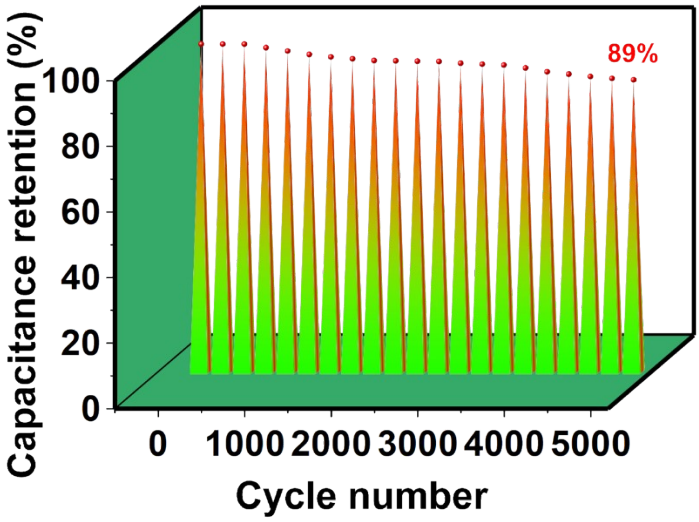

Figure S10. Capacitance retention profile for WMC-2//AC ASC device.

Table S1. Different formats of the three-electrode supercapacitor performance of prepared electrodes

Electrode materials	Applied current ($A \cdot g^{-1}$)	Specific Capacity ($C \cdot g^{-1}$)	Specific capacitance ($F \cdot g^{-1}$)	Specific Capacity ($mAh.g^{-1}$)
$MgFeO_3$	1	168	280	46.6
	2	148	246	41.1
	3	135	225	37.5
	5	125	208	34.7
	10	120	200	33.3
	15	105	175	29.2
	20	90	150	25
$WS_2/MgFeO_3$	1	236	393	65.5
	2	228	380	63.3
	3	213	355	59.2
	5	190	317	52.7
	10	181	300	50
	15	169	282	47.1
	20	160	266	44.4
WMC-1	1	328	546	91.1
	2	308	513	85.6
	3	252	420	70
	5	235	391	65.3
	10	220	366	61.1
	15	183	305	50.8
	20	170	283	47.2
WMC-2	1	420	700	116.6
	2	382	636	106.1
	3	370	620	102.7
	5	350	583	97.2
	10	330	550	91.7
	15	300	500	83.3
	20	282	466	78.3
WMC-3	1	378	630	105
	2	352	586	97.8
	3	330	550	91.6
	5	315	525	87.5
	10	300	500	83.3
	15	265	432	73.6
	20	240	400	66.7

Table S2. Three-electrode **s**upercapacitor performance comparison with various composite electrodes.

Electrode materials	**Electrolyte (M)**	**Specific Capacity / capacitance**	**Capacitance retention (%)/ cycles**	**Ref.**
WMC-2 WS_2/$MgFeO_3$-CNT	***6 M KOH***	***420 C·g^{-1} (700 F·g^{-1}) @ 1 A·g^{-1}***	***93 / 5000***	***In this study***
WS_2/α-$NiMoO_4$ nanocomposite	2 M KOH	460 F·g^{-1} @ 3 A·g^{-1}	92/2000	[1]
$ZnCo_2O_4$/WS_2/FCNTs	3 M KOH	540.5 C/g @ 0.5 A·g^{-1}	86.6/10000	[2]
rGO-MoS_2-WS_2	3 M KOH	365 F·g^{-1} @ 1 A·g^{-1}	-	[3]
MoSSe/CNTs	3 M KOH	512.4 F·g^{-1} @ 1 A·g^{-1}	91.9/3000	[4]
MoS_2/MXene nanohybrid	3 M KOH	583 F·g^{-1} @ 1 A·g^{-1}	82.5/3000	[5]
MoS_2-rGO	1 M Na_2SO_4	387.6 F·g^{-1} @ 3 A·g^{-1}	100/1000	[6]
CZTS/MoS_2/CNT	1 M KOH	273.5 F·g^{-1} @ 1.25 A·g^{-1}	98/1000	[7]
CONi-$CoNiO_2$ nanoparticles	6 M KOH	280 F g^{-1}@ 0.25 A g^{-1}	97.7/10000	[8]
MXene/WS_2-GCE	1 M H_2SO_4	373 F·g^{-1} @ 0.4 A·g^{-}	91.2/1000	[9]
MoS_2/CNS	1 M Na_2SO_4	108 F g^{-1} @ 1 A g^{-1}	-	[10]
$MoSe_2$-Mo_2C hybrid nanoarrays	1 M KOH	850 F·g^{-1} @ 2.5 A·g^{-1}	98/10000	[11]
WS_2/RGO hybrids	1.0 M Na_2SO_4	350 F/g@ 2mV/s	-	[12]
W_2C/MoS_2 hybrid	1 M KOH	681 F·g^{-1} @ 0.5 A·g^{-1}	94/5000	[13]
d-MoS_2/CNT40 heterostructure	1 M KCl	436 F·g^{-1} @ 1 A·g^{-1}	-	[14]
NiO/MoS_2	1 M KOH	289 F g^{-1}@1 A g^{-1}	101.1/2000	[15]
Mn_3O_4/MoS_2	1 M Na_2SO_4	119.3@1 Ag^{-1}	69.3/2000	[16]
VS_2-MXene-CNT	0.5 M K_2SO_4	505.05@ 0.2 Ag^{-1}	-	[17]
$MnCo_2O_{4.5}$@$NiCo_2O_4$ nanowire	3 M KOH	146 C g^{-1} at 5 A g^{-1}	70.5/3000	[18]
$ZnFe_2O_4$-rGO	2 M KOH	352.9 F g^{-1}@1 A g^{-}$_1$	92/10000	[19]
VTe_2/CNT	0.5 m K_2SO_4	255.8 F·g^{-1} @ 1 A·g^{-1}	-	[20]

MoS_2-graphene	1.0 M KOH	756 $F \cdot g^{-1}$ @ 0.5 $A \cdot g^{-1}$	88/10000	[21]
3Dgraphene/ MoS_2 composite	1.0 M Na_2SO_4	410 $F \cdot g^{-1}$ @ 1 $A \cdot g^{-1}$	80.3/10000	[22]
VSe_2/e-MXene/CNT	0.5 M K_2SO_4	182 F g^{-1}@ 1 mA	94.1/5000	[23]
MoS_2-SnS_2	1 M KOH	324 F g^{-1}@ 10 mA	97/4000	[24]
Ti_3C_2Tx/MoS_2	1 M H_2SO_4	595 F g^{-1}@ 1 $A \cdot g^{-1}$	82/2000	[25]
$NiSe_2$@$MoSe_2$/MWCNT	3 M KOH	839 F g^{-1}@ 1 $A \cdot g^{-1}$	96/1000	[26]

Table S3. Two-electrode supercapacitor performances of various composite-based electrodes

Electrode materials	**Electrolyte**	**Specific capacitance**	**Energy density**	**Power density**	**Capacitance retention (%)/cycles**	**Ref.**
WMC-2 WS_2/$MgFeO_3$-CNT	***6 M KOH***	***132 F/g @ 1 A/g^{-1}***	***47 Wh kg^{-1}***	***2250 W kg^{-1}***	***89/5000***	***In this study***
MoSSe/CNTs	3 M KOH	166.5 F g^{-1}@1 A g^{-1}	7.4 Wh Kg^{-1}	3333 W kg^{-1}	96.04/3000	[4]
ZnS@CNT	2 M KOH	231.9 F g^{-1}@1 A g^{-1}	43.3 Wh Kg^{-1}	6.8 kW kg^{-1}	91.79/5000	[27]
$ZnFe_2O_4$-rGO	2 M KOH	33.6 F g^{-1}@0.5 A g^{-1}	6.7 Wh Kg^{-1}	300 W kg^{-1}	-	[19]
$NiMoO_4/Ti_3C_2T_x$	3 M KOH	150 F·g^{-1} @ 1 A·g^{-1}	33.36 Wh/Kg	400.08 W/kg	72.6/10000	[28]
d-MoS_2/CNT40 heterostructure	1 M KCl	164 F·g^{-1} @ 1 A·g^{-1}	27 Wh/Kg	603 W/kg	96/10000	[14]
MXene/$NiCo_2S_4$	6 M KOH	621F·g^{-1} @ 1 A·g^{-1}	72.82 Wh/Kg	0.635k W/Kg	90.88/20000	[29]
VS_2-MXene-CNT	0.5 M K_2SO_4	149.55 F·g^{-1} @ 10 A·g^{-1}	59.85 Wh/Kg	7303.72 W/Kg	93.2/50000	[17]
$NiCo_2$-LDHs@MXene/rGO	3M KOH	240 F·g^{-1} @ 0.5 A·g^{-1}	65.3 Wh/Kg	700 W/kg	92.8/10000	[30]
NiCoS/d-Ti_3C_2	6 M KOH	95.2F·g^{-1} @ 0.5 A·g^{-1}	22.6 Wh/Kg	0.4 kW/kg	91.2/10000	[31]
WS_2@$NiCo_2O_4$/CC	PVA/KOH	196 mF cm^{-2}@ 1 A g^{-1}	45.67 W h kg^{-1}	992.83 W kg^{-1}	85.59/5000	[32]
VTe_2/CNT	0.5 m K_2SO_4	102.04 F·g^{-1} @0.5 A·g^{-1}	36.28 Wh/Kg	463.16 W/kg	80.76/7000	[20]
$Ni_{1.5}Co_{1.5}S_4$-5@Ti_3C_2	6 M KOH	140 A·g^{-1} @ 1 A·g^{-1}	49.8 Wh/Kg	800 W/kg	90/8000	[33]
$WS_2/FeCo_2O_4$	6 M KOH	110 C g^{-1}@ 1A·g^{-1}	85.68 W h kg^{-1}	897.65 W kg^{-1}	98.7%/4000	[34]

WS_2@Ni-Co-S-1	6 M KOH	99.68 $F \cdot g^{-1}$ @ 0.5 $A \cdot g^{-1}$	40.01 Wh· kg^{-1}	417.52 W· kg^{-1}	93/18000	[35]
MXene/CuS	6 M KOH	49.3 $F \cdot g^{-1}$ @ 0.5 $A \cdot g^{-1}$	15.4 Wh/Kg	750.2 W/kg	82.4/5000	[36]
W_2C/MoS_2 hybrid	6 M KOH	121 $F \cdot g^{-1}$ @ 0.5 $A \cdot g^{-1}$	34 Wh kg^{-1}	0.5 kW kg^{-1}	89/5000	[37]

References

[1] S.K. Ray, B. Pant, M. Park, J. Hur, S.W. Lee, Cavity-like hierarchical architecture of WS2/α-NiMoO4 electrodes for supercapacitor application, Ceramics International, 46 (2020) 19022-19027.

[2] M.Z. Khan, M.A. Akram, Z. Ali, M. Mujahid, S. Javed, Mixed morphology ternary composites of ZnCo2O4/WS2/COOH-CNTs for high performance supercapacitor application, Journal of Alloys and Compounds, (2025) 182876.

[3] T.W. Lin, T. Sadhasivam, A.Y. Wang, T.Y. Chen, J.Y. Lin, L.D. Shao, Ternary composite nanosheets with MoS2/WS2/graphene heterostructures as high-performance cathode materials for supercapacitors, ChemElectroChem, 5 (2018) 1024-1031.

[4] J. Liu, B. Gao, D. Xin, M. Ren, Z. Zhu, Y. Zhang, Synthesis of 3D cross-linked MoSSe/CNTs electrode materials for high-stability symmetrical supercapacitors, New Journal of Chemistry, 49 (2025) 19742-19751.

[5] B. Kirubasankar, M. Narayanasamy, J. Yang, M. Han, W. Zhu, Y. Su, S. Angaiah, C. Yan, Construction of heterogeneous 2D layered MoS2/MXene nanohybrid anode material via interstratification process and its synergetic effect for asymmetric supercapacitors, Applied Surface Science, 534 (2020) 147644.

[6] M. Saraf, K. Natarajan, S.M. Mobin, Emerging robust heterostructure of MoS2–rGO for high-performance supercapacitors, ACS applied materials & interfaces, 10 (2018) 16588-16595.

[7] S. Chetana, M. Shetty, V.N. Thakur, M. Ravi, N. Rani, C.A. Kumar, P.D. Shivaramu, D. Rangappa, K.B. Kumar, Ternary Cu2ZnSnS4/MoS2/CNT-Heterostructure as a High-performance Supercapacitor Electrode Material, Journal of The Electrochemical Society, 172 (2025) 123501.

[8] Y. Jiang, Y. Wang, D. Zeng, Y. Xiao, H. Wang, X. Zhang, X. Dai, Synthesis of bimetallic CoNi-CoNiO2 nanoparticles embedded into mesoporous carbon as high-performance catalysts for supercapacitor

electrode, Microporous and Mesoporous Materials, 272 (2018) 222-231.
[9] P.T. Pınar, M. Gülcan, Y. Yardım, Synthesis and characterization of a nanocomposite consisting of Ti3C2Tx (MXene) and WS2 nanosheets for potential use in supercapacitors, Journal of Alloys and Compounds, 1010 (2025) 177656.
[10] T.N. Khawula, K. Raju, P.J. Franklyn, I. Sigalas, K.I. Ozoemena, Symmetric pseudocapacitors based on molybdenum disulfide (MoS 2)-modified carbon nanospheres: correlating physicochemistry and synergistic interaction on energy storage, Journal of Materials Chemistry A, 4 (2016) 6411-6425.
[11] D. Vikraman, S. Hussain, K. Karuppasamy, A. Feroze, A. Kathalingam, A. Sanmugam, S.-H. Chun, J. Jung, H.-S. Kim, Engineering the novel MoSe2-Mo2C hybrid nanoarray electrodes for energy storage and water splitting applications, Applied Catalysis B: Environmental, 264 (2020) 118531.
[12] S. Ratha, C.S. Rout, Supercapacitor electrodes based on layered tungsten disulfide-reduced graphene oxide hybrids synthesized by a facile hydrothermal method, ACS applied materials & interfaces, 5 (2013) 11427-11433.
[13] S. Hussain, I. Rabani, D. Vikraman, A. Feroze, M. Ali, Y.-S. Seo, W. Song, K.-S. An, H.-S. Kim, S.-H. Chun, MoS2@ X2C (X= Mo or W) hybrids for enhanced supercapacitor and hydrogen evolution performances, Chemical Engineering Journal, 421 (2021) 127843.
[14] S. Rani, L. Bansal, R. Bhatia, R. Kumar, I. Sameera, Engineered nano-architecture for enhanced energy storage capabilities of MoS2/CNT-heterostructures: A potential supercapacitor electrode, Journal of Energy Storage, 84 (2024) 110865.
[15] D. Kasinathan, P. Prabhakar, P. Muruganandam, B.R. Wiston, A. Mahalingam, G. Sriram, Solution Processed NiO/MoS2 Heterostructure Nanocomposite for Supercapacitor Electrode Application, Energies, 16 (2022) 335.
[16] M. Wang, H. Fei, P. Zhang, L. Yin, Hierarchically layered MoS2/Mn3O4 hybrid architectures for electrochemical supercapacitors with enhanced performance, Electrochimica Acta, 209 (2016) 389-398.
[17] A. Sharma, C.S. Rout, 1T metallic vanadium disulfide hybridized with MXene and functionalized-MWCNT as a remarkable electrode for high power density asymmetric supercapacitor applications, International Journal of Energy Research, 46 (2022) 24537-24553.
[18] W.C. Huo, X.L. Liu, Y.S. Yuan, N. Li, T. Lan, X.Y. Liu, Y.X. Zhang, Facile synthesis of manganese cobalt oxide/nickel cobalt oxide composites for high-performance supercapacitors, Frontiers in chemistry, 6 (2019) 661.
[19] S. Yang, Z. Han, J. Sun, X. Yang, X. Hu, C. Li, B. Cao, Controllable ZnFe2O4/reduced graphene oxide hybrid for high-performance supercapacitor electrode, Electrochimica Acta, 268 (2018) 20-26.
[20] S.R. Koottumvathukkal Anil, S. Radhakrishnan, N. Kuniyil, J.S. Cho, S.M. Jeong, C.S. Rout, Elucidating the Energy Storage Performance of 2D Metallic Vanadium Ditelluride/Carbon Nanotube for Next-Generation Asymmetric Supercapacitors Using Emerging MoSSe/Carbon Nanotube, Advanced Energy and Sustainability Research, 5 (2024) 2300265.

[21] D. Vikraman, K. Karuppasamy, S. Hussain, A. Kathalingam, A. Sanmugam, J. Jung, H.S. Kim, One-pot facile methodology to synthesize MoS_2-graphene hybrid nanocomposites for supercapacitors with improved electrochemical capacitance, Compos. Part B-Eng., 161 (2019) 555-563.
[22] T. Sun, Z. Li, X. Liu, L. Ma, J. Wang, S. Yang, Facile construction of 3D graphene/MoS_2 composites as advanced electrode materials for supercapacitors, J. Power Sources, 331 (2016) 180-188.
[23] P. Siddu, S.R. KA, S. Radhakrishnan, S. Mun Jeong, C. Sekhar Rout, 3D ternary hybrid of VSe2/e-MXene/CNT with a promising energy storage performance for high performance asymmetric supercapacitor, Batteries & Supercaps, 8 (2025) e202400466.
[24] S. Priya, L. Bharti, S. Shegokar, S. Anshu, D. Mandal, S. Kansal, A. Srivastava, A. Chandra, MoS2-SnS2 composite as electrode material for cost-effective flexible quasi-solid state asymmetric supercapacitor, Journal of Power Sources, 647 (2025) 237298.
[25] N. Tyagi, G. Sharma, M. Khanuja, M.K. Singh, Enhanced supercapacitor performance of Ti3C2Tx/MoS2 heterostructure, Materials Science and Engineering: B, 321 (2025) 118464.
[26] H.S. Shahidani, M. Seifi, M.B. Askari, Design of NiSe2@ MoSe2 nanocomposite anchored on multi-walled carbon nanotubes as advanced supercapacitor applications, Inorganic Chemistry Communications, 170 (2024) 113218.
[27] A. Tamilselvan, S. Sengupta, A. Pramanik, P.M. Ajayan, M. Kundu, Self-assembled ZnS@ CNT composite nanoparticles for advanced supercapacitor electrode, Journal of Materials Science, 60 (2025) 1661-1674.
[28] Y. Wang, J. Sun, X. Qian, Y. Zhang, L. Yu, R. Niu, H. Zhao, J. Zhu, 2D/2D heterostructures of nickel molybdate and MXene with strong coupled synergistic effect towards enhanced supercapacitor performance, Journal of Power Sources, 414 (2019) 540-546.
[29] Y. Li, K. Donatien-Pascal, X. Jin, In situ growth of Chrysanthemum-like NiCo2S4 on MXene for High-performance Supercapacitors and Non-enzymatic H2O2 Sensor, Dalton Transactions, (2020).
[30] J. Zheng, X. Pan, X. Huang, D. Xiong, Y. Shang, X. Li, N. Wang, W.-M. Lau, H.Y. Yang, Integrated MXene-based Aerogel Composite: Componential and Structural Engineering towards Enhanced Performance Stability of Hybrid Supercapacitor, Chemical Engineering Journal, (2020) 125197.
[31] Y. Luo, Y. Tian, Y. Tang, X. Yin, W. Que, 2D hierarchical nickel cobalt sulfides coupled with ultrathin titanium carbide (MXene) nanosheets for hybrid supercapacitors, Journal of Power Sources, 482 228961.
[32] L. Li, J. Gao, V. Cecen, J. Fan, P. Shi, Q. Xu, Y. Min, Hierarchical WS2@ NiCo2O4 Core–shell Heterostructure Arrays Supported on Carbon Cloth as High-Performance Electrodes for Symmetric Flexible Supercapacitors, ACS omega, 5 (2020) 4657-4667.
[33] X. He, T. Bi, X. Zheng, W. Zhu, J. Jiang, Nickel cobalt sulfide nanoparticles grown on titanium carbide MXenes for high-performance supercapacitor, Electrochimica Acta, 332 (2020) 135514.
[34] Y.A. Kumar, G. Mani, M.R. Pallavolu, S. Sambasivam, R.R. Nallapureddy, M. Selvaraj, M. Alfakeer,

A.A.A. Bahajjaj, M. Ouladsmane, S.S. Rao, Facile synthesis of efficient construction of tungsten disulfide/iron cobaltite nanocomposite grown on nickel foam as a battery-type energy material for electrochemical supercapacitors with superior performance, Journal of Colloid and Interface Science, 609 (2022) 434-446.
[35] F. Yang, H. Guo, J. Zhang, N. Wu, M. Yang, Y. Chen, T. Zhang, L. Sun, W. Yang, Core–shell structured WS2@ Ni-Co-S composite and activated carbon derived from rose flowers as high-efficiency hybrid supercapacitor electrodes, Journal of Energy Storage, 54 (2022) 105234.
[36] Z. Pan, F. Cao, X. Hu, X. Ji, A facile method for synthesizing CuS decorated Ti3C2 MXene with enhanced performance for asymmetric supercapacitors, Journal of Materials Chemistry A, 7 (2019) 8984-8992.
[37] S. Hussain, I. Rabani, D. Vikraman, A. Feroze, M. Ali, Y.-S. Seo, W. Song, K.-S. An, H.-S. Kim, S.-H. Chun, MoS2@ X2C (X= Mo or W) hybrids for enhanced supercapacitor and hydrogen evolution performances, Chemical Engineering Journal, (2020) 127843.